Coronagraphs adapted to atmosphere conditions

Miguel A. Cagigas, Pedro J. Valle,* and Manuel P. Cagigal

Departamento de Física Aplicada, Universidad de Cantabria, Avenida de los Castros s/n, 39005 Santander, Spain
**vallep@unican.es*

Abstract: In this paper we show new ways to improve the performance of ground-based coronagraphy. We introduce adaptive coronagraphic masks whose profile is a binary version of the instantaneous atmospherically degraded star image. We also propose the hyper-Gaussian profile masks obtained by averaging adaptive masks. In addition, adaptive Lyot stops and hyper-Gaussian Lyot stops are analyzed. Computer simulations show that all these masks outperform the circular hard-edged mask and that a proper mask and stop combination significantly reduces the angular separation at which a faint companion can be detected.

OCIS codes: (350.1260) Astronomical optics; (110.6770) Telescopes; (100.2980) Image enhancement; (110.2970) Image detection systems.

References and links

1. O. Guyon, E. A. Pluzhnik, R. Galicher, F. Martinache, S. T. Ridgway, and R. A. Woodruff, "Exoplanet imaging with a phase-induced amplitude apodization coronagraph. I. Principle," Astrophys. J. **622**(1), 744–758 (2005).
2. D. Rouan, D. Riaud, A. Boccaletti, Y. Clénet, and A. Labeyrie, "The four-quadrant phase-mask coronagraph," Publ. Astron. Soc. Pac. **112**(777), 1479–1486 (2000).
3. M. J. Kuchner and W. A. Traub, "A coronagraph with a band-limited mask for finding terrestrial planets," Astrophys. J. **570**(2), 900–908 (2002).
4. J. E. Oti, V. F. Canales, and M. P. Cagigal, "Pure amplitude masks for exoplanet detection with the Optical Differentiation Coronagraph," Astrophys. J. **662**(1), 738–743 (2007).
5. A. Ferrari, R. Soummer, and C. Aime, "An introduction to stellar coronagraphy," C. R. Phys. **8**(3-4), 277–287 (2007).
6. O. Guyon, E. A. Pluzhnik, M. J. Kuchner, B. Collins, and S. T. Ridgway, "Theoretical limits on extrasolar planets detection with coronagraphs," Astrophys. J. Suppl. Ser. **167**(1), 81–99 (2006).
7. V. F. Canales and M. P. Cagigal, "Gain estimate for exoplanet detection with adaptive optics," Astron. Astrophys. **145**, 445–449 (2000).
8. E. Serabyn, K. Wallace, M. Troy, B. Mennesson, P. Haguenauer, R. Gappinger, and R. Burruss, "Extreme adaptive optics imaging with a clear and well-corrected off-axis telescope subaperture," Astrophys. J. **658**(2), 1386–1391 (2007).
9. L. A. Poyneer and B. Macintosh, "Spatially filtered wave-front sensor for high-order adaptive optics," J. Opt. Soc. Am. A **21**(5), 810–819 (2004).
10. M. P. Cagigal and V. F. Canales, "Generalized Fried parameter after adaptive optics partial wavefront compensation," J. Opt. Soc. Am. A **17**(5), 903–910 (2000).
11. P. Bourget, R. Vieira Martins, F. Colas, P. Assus, and A. Irbah, "Adaptive mask coronagraph," in *Direct Imaging of Exoplanets, Science and Techniques*, C. Aime and F. Vakili eds. (Cambridge University Press, 2006), pp. 461–465.
12. See for example: http://www.ti.com/lit/ds/symlink/dlp5500.pdf.
13. M. Lacolle, R. Belikov, H. Sagberg, O. Solgaard, and A. S. Sudbø, "Algorithms for the synthesis of complex-value spectral filters with an array of micromechanical mirrors," Opt. Express **14**(26), 12590–12612 (2006).
14. L. Labadie, R. Rebolo, L. Villó, J. A. Pérez Prieto, A. Pérez-Garrido, S. R. Hildebrandt, B. Femenia, A. Díaz-Sanchez, V. J. S. Bejar, A. Oscoz, R. Lopez, J. Piqueras, and L. F. Rodríguez, "High-contrast optical imaging of companions: the case of the brown dwarf binary HD 130948 BC," Astron. Astrophys. **526**, A144 (2011).
15. N. Roddier, "Atmospheric wavefront simulation using Zernike polynomials," Opt. Eng. **29**(10), 1174–1180 (1990).
16. J. R. Crepp, A. D. Vanden Heuvel, and J. Ge, "Comparative Lyot coronagraphy with extreme adaptive optics systems," Astrophys. J. **661**(2), 1323–1331 (2007).
17. J. W. Hardy, *Adaptive Optics for Astronomical Telescopes* (Oxford University Press, 1998).
18. S. B. Shaklan and J. J. Green, "Low-order aberration sensitivity of eighth-order coronagraph masks," Astrophys. J. **628**(1), 474–477 (2005).
19. M. J. Kuchner and D. N. Spergel, "Notch filter masks: Practical image masks for planet-finding coronagraphs," Astrophys. J. **594**(1), 617–626 (2003).
20. M. Kowalczyk, T. Cichocki, M. Martinez-Corral, and V. Kober, "Binarization of continuous-tone pupil filters: a comparison of several digital halftoning procedures," Pure Appl. Opt. **4**(5), 553–570 (1995).

#156870 - $15.00 USD Received 24 Oct 2011; revised 27 Dec 2011; accepted 22 Jan 2012; published 9 Feb 2012

21. P. Martinez, C. Dorrer, and M. Kasper, "Band-limited coronagraphs using halftone dot process: design guidelines, manufacturing and laboratory results," Astrophys. J. **705**(2), 1637–1645 (2009).

1. Introduction

Among the different techniques proposed for direct detection of earth-like exoplanets (planets outside our solar system), Lyot coronagraphy is particularly attractive because of its simplicity and good performance. From the original Lyot coronagraph, different improving designs like the pupil reshaping [1] or the use of sophisticated phase [2] or amplitude mask [3,4] have been introduced. A thorough review can be found in Refs [5,6].

The coronagraph is a static instrument that produces a high star light extinction without affecting faint companion light. However, the phase distortion introduced by atmospheric turbulence affects the attainable extinction rate to a great extent so that the employ of sophisticated masks becomes almost useless. This effect becomes more important when the ratio between the telescope pupil entrance diameter (D) and the atmosphere Fried parameter (r_0) increases, since the wavefront phase variance scales as $(D/r_0)^{5/3}$. A ground-based coronagraph would require extreme adaptive optics to achieve its best performance [7]. Currently, much effort is being done on this topic [8,9].

In this paper we propose new types of coronagraphic masks and stops that take into account the wavefront distortions caused by the atmosphere. Our goal is not to use highly compensated wavefronts to detect objects very close to the main star but to use uncompensated wavefronts to detect them a little further. The expected science of this proposal is not the same as that of coronagraphy using extreme adaptive optics but it is complementary and technically more affordable.

We introduce adaptive coronagraphic masks whose shapes evolve with the speckled star image. We also obtain average masks from the set of adaptive masks. These average masks are fitted by hyper-Gaussian profiles and then binarized using different algorithms. Description, analysis and performance comparison are carried out for all mask types and for different atmosphere conditions. Adaptive, average adaptive and hyper-Gaussian Lyot stops are also introduced. Finally, the combination of different coronagraphic masks and Lyot stops are checked and their results are compared for different star-companion intensity ratios.

2. Adaptive coronagraphic masks

In a ground-based telescope the Point Spread Function (PSF) is composed of a coherent peak and a surrounding speckled halo dynamically changing with atmospheric seeing variation [10]. Hence, an efficient light extinction could be performed using an adaptive coronagraphic mask (AM) able to cancel out not only the central PSF core but also the most brilliant part of the surrounding speckled halo. Although a circular mask that changes its radius as a function of seeing has already been used [11], no conclusive results were reported. The adaptive masks here proposed will dynamically change not only its size but also its shape as a consequence of the seeing temporal evolution.

Figure 1(a) sketches a classical Lyot coronagraph but using an adaptive mask, AM. In this setup a beam splitter (BS) sends a fraction of the incoming star light to a CCD camera to form an image of the instantaneous PSF. The registered PSF is then binarized by applying a certain threshold. Pixels with intensity values above the threshold will provide the dark points of the mask (tilted micro-mirrors as describes here after). The adaptive mask shape will be the binary version of the instantaneous PSF. The light passing through the BS produces the masked star light by reflection on the AM device with the mask shape information encoded on it. As an example, Fig. 1(b) shows a transversal cut of the star (blue) and companion (red) PSFs along with the threshold value (horizontal green line). A detail of the resulting binary mask is shown in Fig. 1(c) (see next section for simulation details).

To perform the binary reflective device of the AM we suggest the use of an array of micro-mirrors since every micro-mirror can be independently tilted at very high speed (several kHz) [12,13]. An exact correspondence between pixels at the CCD camera and micro-mirrors of the adaptive mask is required. Currently, the micro-mirror size is about 12

#156870 - $15.00 USD Received 24 Oct 2011; revised 27 Dec 2011; accepted 22 Jan 2012; published 9 Feb 2012

μm. Since atmospheric fluctuations take between 10 ms and 50 ms to occur (I band), an appropriate sample rate could be around 30 ms what allows a good balance between the need of freezing the atmosphere and the need of a high signal to noise ratio. Similar rate values have been successfully used in Lucky Imaging techniques [14].

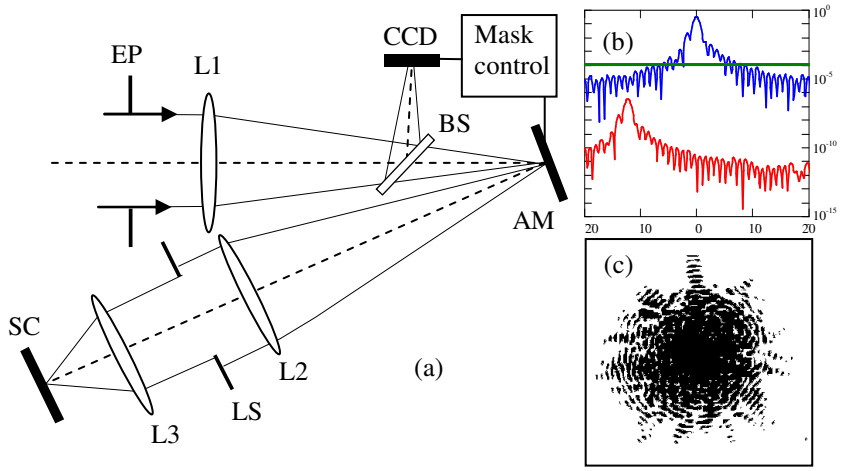

Fig. 1. (a) Adaptive coronagraph. EP: Entrance pupil, L1: Telescope primary mirror, BS: Beam Splitter, CCD: Camera, AM: Reflecting adaptive mask, L2 and L3: 4-f system, LS: Lyot stop, and SC: Scientific camera. (b) Transversal cut (λ/D in units) of the star PSF (blue line) and the threshold used to determine the adaptive mask shape (green line). The companion PSF (red line) is below the threshold. (c) Detail of a binary adaptive mask obtained from the star PSF.

3. Numerical simulation

We have studied the AM performance by numerical simulation in the framework of the Fourier Optics. The field at the telescope entrance pupil is expressed as $E(x,y) = exp(i\Phi(x,y))$, where $\Phi(x,y)$ is the wavefront aberration function, x and y are the spatial Cartesian coordinates and a constant field amplitude is assumed. This field is Fourier transformed to simulate the telescope outcome and multiplied by the coronagraphic mask. The product is again transformed and multiplied by the Lyot stop. Finally, a third Fourier Transform is calculated to form the final image.

Computer simulations were carried out using the FFT routine implemented in Matlab. To achieve a good spatial sampling and to avoid aliasing effects, 1024x1024 data samples were used. The telescope pupil (EP in Fig. 1) was simulated with a 128x128 data sampling. The hard-edged Lyot (HEL) stop was set to the 75% of the telescope aperture radius. The size of the Lyot stop will remain unchanged up to Section 6. We simulated series of $\Phi(x,y)$ for a number of atmospheric conditions following the standard procedure established by Roddier [15]. In all cases piston, tip and tilt were corrected. We also considered a faint companion object whose intensity was 10^6 times smaller than that of the main star.

The key parameter chosen to determine the masks performances was the smallest angular separation at which the faint companion can be detected (ρ). We considered that an object can be detected when the intensity ratio between the object and the remaining star halo is larger than 5 (SNR_{CS}>5). Since the companion light intensity is almost unaffected by the coronagraph, the companion would be detected at those positions at which the star halo is around five times smaller than the intensity companion.

Although, the circular hard-edged mask (HEM) is the best performing option for uncompensated ground-based detection, as it was shown by Crepp et al [16], we compared AM results with those of the HEM and 4th-order band limited masks (BLM). We considered those cases in which the coherent peak intensity contributes to the Strehl ratio more than the

#156870 - $15.00 USD Received 24 Oct 2011; revised 27 Dec 2011; accepted 22 Jan 2012; published 9 Feb 2012

halo peak intensity. Since this happens for $D/r_0 < 7.8$ [17], we analyzed up to $D/r_0 \leq 7$. Otherwise, speckle peaks could have so low values that the resulting AM would cover almost completely the coronagraphic mask plane and therefore also blocking the exoplanet light.

4. Adaptive and hard-edged coronagraphic mask comparison

The first step was to determine the optimum HEM for the different atmospheric seeing conditions. For this purpose a set of one hundred images were obtained from the corresponding wavefront realizations for a particular D/r_0 value and a particular HEM radius. Then the calculated average image was used to determine the angular separation ρ_{HE} at which $SNR_{CS}>5$. The process was repeated for different HEM radii and we choose those radii providing the smallest ρ_{HE}. The so obtained HEM radii were 10, 14, 18 and 22 (in λ/D units) for D/r_0 = 1, 3, 5 and 7 respectively. Since the IWA is defined as the halfwidth at half-maximum of the intensity transmission profile, IWA and radii values are the same as it is shown in Table 1. Figure 2(a) (blue line) shows values of ρ_{HE} obtained for the best performing HEM for atmosphere condition in the range $D/r_0 \leq 7$. Figure 3(left) shows an average image calculated for $D/r_0 = 3$.

Table 1. IWA Values* of HEM, HGM and BLM for D/r_0 = 1, 3, 5, and 7

D/r_0	1	3	5	7
HEM	10	14	18	22
HGM	9.6	14	18	23
BLM	8.5	14	21	31

*IWA values in λ/D units.

The second step was to determine the AM that provides the smallest angular separation ρ_{AM} at which $SNR_{CS}>5$. We checked different criteria to establish the mask threshold. The selected criterion was the percentage of the star light blocked by the mask. We applied the threshold needed to attain a particular blocked energy value to every wavefront realization. The angular separation ρ_{AM} was estimated from the average of the set of final images. The whole process was repeated for blocked energy values ranging in the interval 97%-99%. The optimal blocked energy values were those providing the smallest ρ_{AM} (Fig. 3 (centre) shows an example of average image for $D/r_0 = 3$).

We found out an empirical relation for the dependence of the optimal value of the blocked energy (*BE*, in percent) with D/r_0:

$$BE = 97.5 + 0.25(D / r_0)^{5/6} . \quad (1)$$

This equation allows evaluating the AM in an actual experiment. Figure 2(a) shows the values of ρ_{AM} (green line) along with those of ρ_{HE} (blue line) as a function of D/r_0. It can be seen that ρ_{AM} values are always smaller than ρ_{HE} ones. The angular separation reduction in percent is evaluated through:

$$\Delta\rho = \frac{\rho_{HE} - \rho_{AM}}{\rho_{HE}} 100 . \quad (2)$$

Figure 2(b) shows $\Delta\rho$ as a function of D/r_0. It can be seen that the AM (green line) produces an angular separation reduction ranging from 3% to 9%. The gain of AM over the HEM becomes interesting only for reasonably good atmospheric conditions, as for example $D/r_0 = 1$ where the gain is almost 10%. Finally, an additional advantage of adaptive masks is they are not sensitive to pointing errors since its shape evolves as the star PSF does.

#156870 - $15.00 USD Received 24 Oct 2011; revised 27 Dec 2011; accepted 22 Jan 2012; published 9 Feb 2012

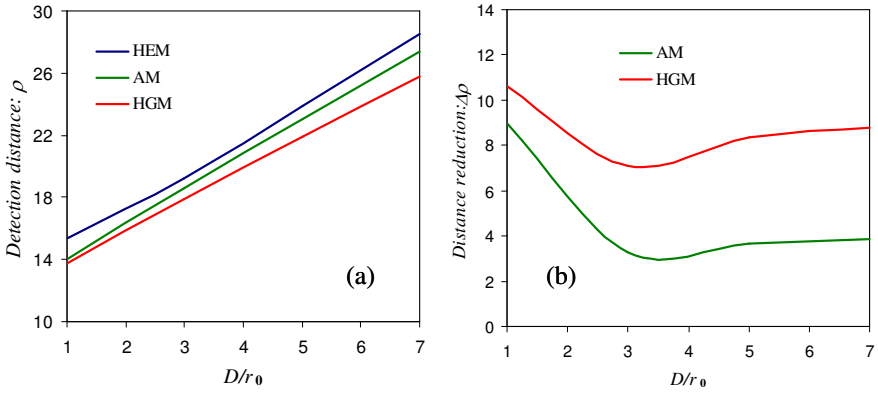

Fig. 2. (a) Values of the angular separation ρ (λ/D units) from the star to the nearest point in which $SNR_{CS}>5$ as a function of D/r_0. (b) Percentage value $\Delta\rho$ following Eq. (2). Blue, green and red lines are for HEM, AM and HGM respectively.

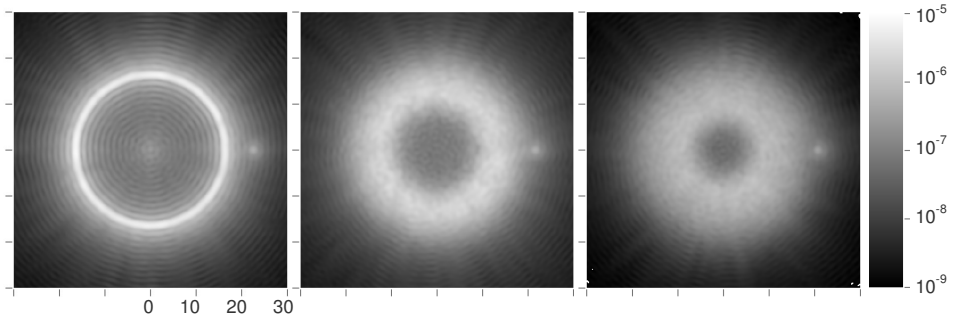

Fig. 3. Final average image for HEM (left), AM (centre) and HGM (right) for $D/r_0 = 3$. The companion positions are 22, 23 and 24 λ/D, respectively, so that in all cases the condition $SNR_{CS}>5$ is fulfilled.

5. Hyper-Gaussian coronagraphic masks

In the previous section, the masks performance analysis has been carried out by averaging a set of scientific camera images corresponding to different atmosphere realizations. Image averaging implies not only the average of different atmosphere realization but also of different AM shapes. We decided to obtain an average AM by averaging the set of one hundred optimum masks corresponding to set of atmosphere realization. This process was repeated for every D/r0 value. The advantage of using an average AM is that it makes the PSF sensor and the micro-mirrors array to be unnecessary.

Average masks obtained by this procedure are no longer binary but their sizes still depend on D/r_0. The profile of these masks can be fitted in all cases by a 4^{th}-order hyper-Gaussian function with a high regression coefficient:

$$HG(r) = 1 - \exp\left[-\frac{r^4}{\sigma^4}\right], \tag{3}$$

where r is the radial coordinate. The evolution of the parameter σ (hyper-Gaussian width in λ/D units) is linear with D/r_0, and it can be expressed as:

$$s = 2.40\left(D / r_0\right) + 8.15. \tag{4}$$

#156870 - $15.00 USD Received 24 Oct 2011; revised 27 Dec 2011; accepted 22 Jan 2012; published 9 Feb 2012

Hence, we will use the hyper-Gaussian function given by Eqs. (3) and (4) instead of average masks. Hyper-Gaussian functions belong to the family of band-limited ones, as it can be seen in Ref [18]. It is interesting to note that the shape of these hyper-Gaussian masks (HGM) derives from the statistics of the speckled light in the star PSF. Consequently, the mask selection will depend on the site seeing and size of the telescope pupil entrance. IWA values of HGM calculated multiplying σ by the factor 0.91 are shown in Table 1.

A wavefront series was simulated for every D/r_0 value. The HGM was applied to every wavefront of the series. The set of final images obtained by this procedure were averaged. Then the angular separation ρ_{HG} corresponding to nearest point in which $SNR_{CS}>5$ was estimated (an example of average image using HGM is shown in Fig. 3(right) for $D/r_0 = 3$).

Figure 2(a) shows the values of ρ_{HG} (red line) as a function of D/r_0. The ρ_{HG} values are smaller than those obtained using HEM and AM. Figure 2(b) shows the $\Delta\rho$ comparison between HGM and AM. The HGM (ranging from 7% to 11%) produces larger angular separation reduction than AM. In principle, these masks have a clear advantage since they do not need instantaneous PSF sensor and adaptive mask devices. However, it is mandatory the use of a tip-tilt compensation system to take full advantage of them.

The contrast profile is a useful tool to compare masks performances and it is defined as:

$$C(r) = \frac{I(r)}{I_s(0)\left|M(r)\right|^2}, \tag{5}$$

where $I(r)$ is the intensity at the radial coordinate in the final image, $I_s(0)$ is the peak stellar intensity measured without the image mask in the optical train and $|M(r)|^2$ is the mask intensity transmission. To compare our results with those of a standard 4^{th}-order band-limited mask we used a mask function [3]:

$$BLM(r) = 1 - sinc^2(\gamma r), \tag{6}$$

where the value of γ has been selected to force the mask to reject the same energy as HEM and HGM for every D/r_0 value. Table 1 shows that the IWA value of BLM is smaller than those of HEM and HEM for low D/r_0. However, when D/r_0 increases, the IWA of BLM increases more quickly than the others. Figure 4 shows the contrast profile for HEM, HGM and BLM and a Lyot fixed at 75% throughput together with the final star intensity calculated without mask and Lyot at 100% throughput. The HGM improves the contrast of HEM and BLM for all the D/r_0 analyzed and the difference increases with the distance. Therefore, the angular separation reduction is more significant when detecting faint objects since the condition $SNR_{CS}>5$ takes place far from the star. The contrast improvement offered by HGM can be understood in terms of they are designed for dealing with aberrated wavefronts whilst BLM are designed to cancel out light coming from a perfect wavefront.

A drawback of continuous mask is that they are difficult to be manufactured. Hence, we checked different algorithms to binarize the HGMs [19–21]. The best results were obtained applying the Error Diffusion Algorithm. Binarized hyper-Gaussian masks provide basically the same results as HGMs. This makes the use of HGM a realistic option to improve ground-based coronagraph performances since they are cheaper and simpler to be implemented.

6. Adaptive Lyot stops

So far, we have assumed hard-edged Lyot stops (HEL) set to the 75% of the telescope aperture radius. As it was carried out for the coronagraphic masks, it is possible to define adaptive (AL) and hyper-Gaussian (HGL) Lyot stops. AL stop could be experimentally implemented using the same technique that was proposed for the AM mask. Continuous hyper-Gaussian profiled transmission filters could be used as a HGL. These new Lyot stops can be combined with the preceding coronagraphic masks. The criterion to obtain the thresholds for AL stops was to block the same area as a HEL with 75% telescope aperture radius. The set of AL stops so obtained was averaged and a 4th-order hyper-Gaussian profile

#156870 - $15.00 USD Received 24 Oct 2011; revised 27 Dec 2011; accepted 22 Jan 2012; published 9 Feb 2012

was fitted to it (HGL). Although the use of this HGL will slightly modify the PSF companion shape we are dealing with D/r_0 large enough to produce speckled PSF, so speckle will dominate the PSF shape (except for $D/r_0 = 1$).

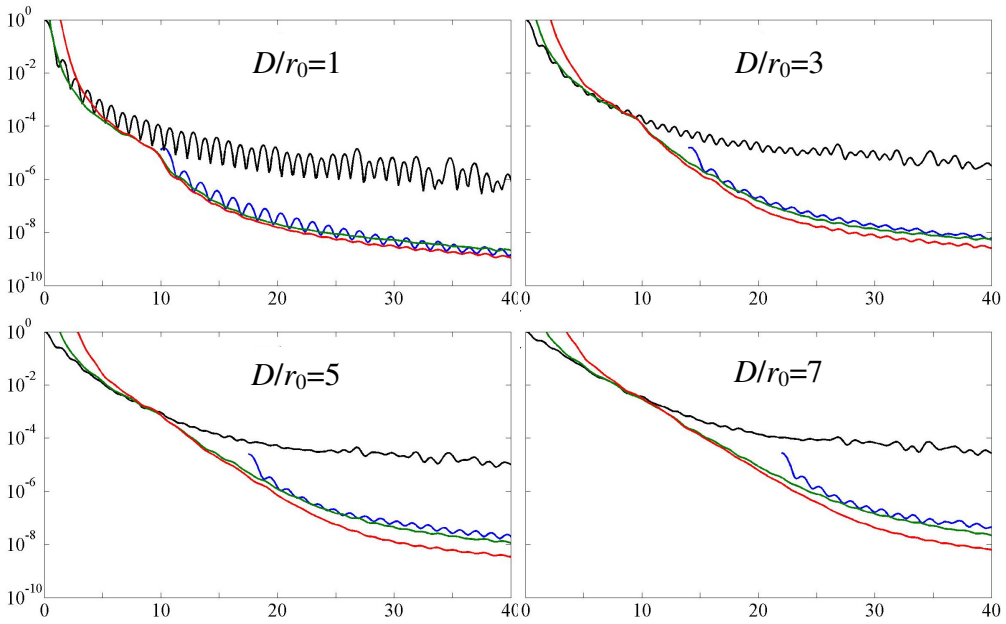

Fig. 4. Aberrated Airy pattern (black) and averaged contrast curves for the HEM (blue), HGM (red), and BLM (green) masks for a fixed circular Lyot stop size with 75% throughput. Abscissa axis is the radial coordinate in λ/D units.

Table 2. Combinations of Masks and Lyot Stops; Star-Companion Intensity Ratio: 10^6*

Δρ % (I/I_{HE})	HEM	AM	HGM
HEL	- (1.0)	9.0 (1.0)	10.6 (0.9)
	- (1.0)	3.3 (1.0)	7.1 (0.7)
	- (1.0)	3.7 (1.0)	8.4 (0.6)
	- (1.0)	3.9 (1.0)	9.0 (0.5)
AL	7.4 (0.8)	9.8 (0.8)	14.7 (0.8)
	3.9 (0.8)	5.2 (0.8)	10.4 (0.6)
	4.7 (0.8)	5.8 (0.8)	11.0 (0.5)
	5.3 (0.8)	6.7 (0.8)	11.9 (0.3)
HGL	16.3 (0.5)	17.1 (0.5)	18.0 (0.4)
	11.1 (0.5)	11.7 (0.3)	12.3 (0.3)
	12.6 (0.5)	12.9 (0.5)	13.1 (0.2)
	13.2 (0.5)	14.4 (0.5)	14.5 (0.1)

*Angular separation reduction in percent and normalized companion intensity in parentheses for D/r_0 values of 1 (green), 3 (red), 5 (blue) and 7 (black).

The new Lyot stops were combined with the HEM, AM and HGM for every D/r_0 value. Table 2 shows the angular separation reduction in percent ($\Delta\rho$) for D/r_0 = 1, 3, 5 and 7 (green, red, blue and black figures, respectively). It can be seen that HGL stops outperform AL and HEL ones for all mask types. Hence, a general conclusion is that all combinations outperform the pair of hard-edged mask and stop and the best results correspond to mask and stop having hyper-Gaussian profiles. It is interesting to note that with only changing the HEL to HGL the

#156870 - $15.00 USD Received 24 Oct 2011; revised 27 Dec 2011; accepted 22 Jan 2012; published 9 Feb 2012

results obtained are very close to the best ones. Therefore, it appears to be more effective a proper Lyot stop selection than a coronagraphic mask selection.

Another feature to be taken into account is how different masks and stops affect the intensity of the star companion object. Table 2 shows in parenthesis companion intensity values, normalized to those obtained using HEM and HEL. It can be seen that the mask and stop combinations producing the larger angular separation reduction lead to an attenuation of the companion intensity. This attenuation can be significant for the case of HGM and HGL. Hence, the use of AM and AL is the best option in those cases in which a balance between the detection angular distance reduction and the intensity companion attenuation is an essential issue.

Table 3. Combinations of Masks and Lyot Stops; Star-Companion Intensity Ratio: 10^{7*}

$\Delta\rho$ % (I/I_{HE})	HEM	AM	HGM
HEL	- (1.0)	14.5 (1.0)	18.2 (1.0)
	- (1.0)	7.3 (1.0)	14.6 (1.0)
	- (1.0)	14.1 (1.0)	26.5 (1.0)
	- (1.0)	19.4 (1.0)	30.5 (0.9)
HGL	34.2 (0.5)	34.8 (0.5)	35.3 (0.5)
	23.0 (0.5)	23.3 (0.5)	26.0 (0.4)
	30.2 (0.5)	31.5 (0.4)	33.6 (0.4)
	34.1 (0.5)	34.6 (0.5)	36.3 (0.4)

*Angular separation reduction in percent and normalized companion intensity in parentheses for D/r_0 values of 1 (green), 3 (red), 5 (blue) and 7 (black).

7. Influence of the star-companion intensity ratio

As it can be seen in the contrast profiles (Fig. 4), the coronagraph performance depends in a great extent on the companion position and intensity. In fact, when the star-companion intensity ratio is 10^5, the best results correspond to hard-edged mask and stop. However, when the ratio is 10^6, the coronagraph performance is strongly dependent on the mask and stop used, as it was shown in Table 2. Results for a star-companion intensity ratio of 10^7 are depicted in Table 3 (except for the AL cases). A relevant angular separation reduction is attained for all mask and stop combinations. In particular the combination HGM and HGL provides an angular separation reduction ($\Delta\rho$) around 30% for $D/r_0 = 5$, which is more than twice that obtained for the ratio of 10^6. In addition, the companion intensity attenuation produced by the coronagraph is smaller than in Table 2 (values in parentheses), so that an important reduction of the detection angular separation can be reached with a little intensity companion attenuation. For a ratio of 10^8 results are even improved. As an example, the detection angular separation reduction overcomes 60% for HGM and HGL combination. This result is a consequence of that both AM and HGM masks reduce the star halo more efficiently in the outermost area than in the innermost area. Hence, when the companion intensity decreases the detection angular separation increases and precisely at these long angular separations the AM and HGM are more efficient. This provokes a significant $\Delta\rho$ increase.

8. Conclusions

In this paper we propose new approaches to improve ground-based coronagraphy for moderately aberrated wavefronts ($D/r_0 \leq 7$). We first developed the adaptive masks whose shape changes to occlude a fixed percentage of the star speckled PSF intensity. This kind of masks allows an object to be detected at a closer angular separation than with the hard-edged mask. An additional advantage is they are not sensitive to pointing errors. We also used hyper-Gaussian masks obtained by averaging adaptive masks. Hyper-Gaussian masks perform better than adaptive ones. Binarized hyper-Gaussian masks produce the same results as the continuous profiles though they are easier to be manufactured. We also defined adaptive and

#156870 - $15.00 USD Received 24 Oct 2011; revised 27 Dec 2011; accepted 22 Jan 2012; published 9 Feb 2012

hyper-Gaussian Lyot stops. These stops also improve the results of standard hard-edged Lyot stop.

We combined the different masks and stops and found that all of them outperform the standard coronagraph. In particular, the best results were obtained for hyper-Gaussian coronagraphic mask and Lyot stop. However, this filter combination leads to the attenuation of the companion intensity. A balance between detection angular separation reduction and companion intensity attenuation can be reached using adaptive mask and stop.

Finally, it can be seen from the contrast profiles that the reduction of the detection angular separation is more relevant for fainter companions since in these cases the condition $SNR_{CS}>5$ takes place far from the star.

Acknowledgments

This work was supported by the Ministerio de Ciencia e Innovación, under project AYA2010-19506. We would like to sincerely thank the valuable comments of the referees which helped us to improve the manuscript.

#156870 - $15.00 USD Received 24 Oct 2011; revised 27 Dec 2011; accepted 22 Jan 2012; published 9 Feb 2012